Accepted article (AMC2018)

Experimental framework of traveling trolley with swinging load for hybrid motion control

Wais Karimi, Michael Ruderman
Department of Engineering Science
University of Agder
Post box 422, 4604-Kristiansand, Norway

Kenta Seki, Makoto Iwasaki
Department of Computer Science and Engineering
Nagoya Institute of Technology
Gokiso, Showa, Nagoya, 466-8555, Japan

***Abstract*—A novel experimental framework of the traveling trolley with swinging load is proposed. The system is designed as a controlled moving cart with pendulum for investigation of the hybrid motion control methods, involving the discrete sensors and impulsive event-based state observations and control actions. A mechatronic approach of principal system design, modeling, and identification are provided together with a motion control of the cart and simple event-based control of a-priori unknown final position. The coupled motion dynamics is analyzed and evaluated by using the discrete sensors, along with the control results.**

I. Introduction

Hybrid control systems [1], [2], as whole, consider the discrete sensing and state transitions, correspondingly control actions, simultaneously with the continuous dynamics which are traditionally assumed in the control theory. Discrete sensors, often as more robust and less expansive comparing to the devices used for measuring the continuous quantities, are widely used in hybrid system applications like embedded systems, controlled hierarchical equipment, complex multi-DOF mechatronic systems and others. Inherent drawback of the discrete sensors is, however, their binary-valued observation anchored to a certain threshold (level) of the measured continuous state. Beyond this threshold no consecutive measurements are available. A methodology for state estimation of hybrid systems with the discrete sensors can be found e.g. in [3]. However their use in motion control applications is rather rare.

Traveling trolley with a swinging load constitutes an aggregating class of under-actuated dynamic systems for which various applications can be found in the cargo logistics, marine and offshore industries, production lines and others. For instance, the overhead cranes have been always challenging for fast motion control with minimization of a parasitic load swinging, once a robust and time-optimal transfer of the payloads is required, see e.g. [4], [5], [6], [7]. An overview with references on the control strategies of crane systems can be found e.g. in [8]. A robust external sensing of the swinging load, either placed on the moving trolley or decoupled from that, is still in focus of system and control design so as to allow for a reliable and feedback-suitable state observation. For example, a visual tracking system of the moving overhead crane load can be found in [9]. On the other hand, the hybrid motion control approaches, incorporating the decoupled external digital sensors and associated event-based discrete control co-actions, appear promising for cranes and other swinging load applications.

In this paper, we introduce a novel experimental framework which allows investigating the under-actuated dynamics of a swinging load hanging on the traveling trolley, and developing the hybrid control methods with involvement of external digital sensors. The use of robust and less expensive binary sensors, decoupled from the traveling trolley, offers additional possibilities in the state estimation of a swinging load, and extension of the standard motion control techniques to those with event-based hybrid approach. Several aspects of system design, identifiability, and controllability are in focus of the proof of concept and experimental framework development.

The rest of the paper is organized as following. In Section II, the mechatronic design is described with a given system overview. Section III is devoted to identification and final tuning of the system parameters. The control design of the cart position tracking is summarized in Section IV. Final model and control evaluation with experiments are shown in Section V, also including effects of variable payload on the system dynamics. The event-based hybrid control approach is given in Section VI. The final conclusions are drawn in Section VII.

II. Design of Experimental Setup

The mechatronic design of a down-scaled testbed of the traveling trolley is achieved by combining a standard ball-screw drive [10] with the newly designed pendulum system. The pendulum system is conceptualized in accord with the desired requirements on the oscillation period and maximal allowed mass to be put on the ball-screw. In order to keep the system dynamics high as possible, the total payload of the ball-screw drive is limited to $5\,kg$, as one of the design criteria. The desired oscillation period is set to be about $1\,s$. The final CAD-based design is made so as to fulfill the dynamics requirements, but also simplicity and overall functionality of the system. The system consists mainly of the following components: (i) support column, (ii) pendulum bearing, (iii) pendulum rod, (iv) load discs, (v) discrete sensors, and (vi) ball-screw drive, all shown in Fig. 1. The support column is a binding component between the actuator system and pendulum, and it is made of aluminum to keep the total weight possibly low. Moreover, the pivoting is achieved by using the Y-bearing units (from SKF Inc), selected due to its small bore diameters, cost effectiveness, and versatility. Note that the pivoting point of pendulum is also a critical point for the swinging dynamics. It is important to keep the frictional torque possibly low so as to achieve a reasonably high number of free oscillations and, therefore, to be able to emulate the free swinging of a hanging load. Thus, the bearing arrangement and quantity have been considered and analyzed before finalizing the design.

© 20XX IEEE. Personal use of this material is permitted. Permission from IEEE must be obtained for all other uses, in any current or future media, including reprinting/republishing this material for advertising or promotional purposes, creating new collective works, for resale or redistribution to servers or lists, or reuse of any copyrighted component of this work in other works.

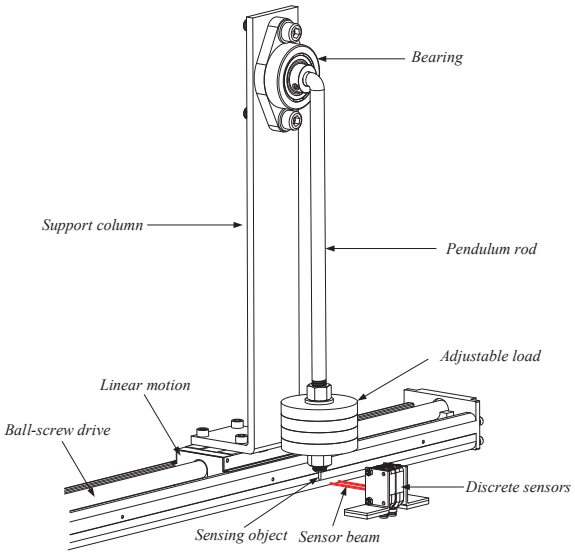

Fig. 1. Experimental setup with designed components

In a numerical simulation, the swinging load is modeled as a simple physical pendulum while the mass of the rod is also taken into consideration. The pendulum consists of a load mass m_l and rod with mass m_r and length l. The pendulum rod is dimensioned based on the requirement of oscillation period. MATLAB scripts are used to evaluate the pendulum dynamics and, therefore, determine the system parameters m_l, m_r, and l. The load is adjustable by means of 4 mass discs, each one about $0.25\,kg$. Note that an adjustable mass is required for studying the variable payloads affecting the overall system dynamics. The laboratory setup of the constructed system of traveling trolley with the swinging load is shown in Fig. 2.

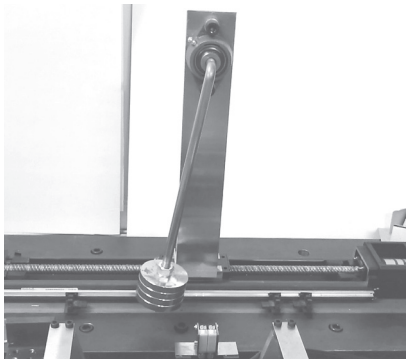

Fig. 2. Laboratory view of the assembled experimental setup

Two photoelectric sensors are used for a discrete detection of vertical position of the pendulum rod and online estimation of tangential velocity when swinging. The selected sensors' switching frequency of $1650\,Hz$ is relatively high, comparing to the system time constants. The sensors have also background suppression ability, that means they are distance-setable. For accurate detection of the vertical position of pendulum rod an additional screw is mounted on the bottom end of the rod. This provides a detection range of $\pm 4°$ around vertical position.

III. System identification and parameters estimation

The overall flowchart of system identification following by the control design is schematically shown in Fig. 3. Model structure is obtained by using the Newton's law of motion. Further, experiments are carried out to obtain the system frequency response. The identified model is then compared with the measured frequency response. Moreover, the system parameters are estimated and, based thereupon, the control system is designed. Finally, the model and controller are validated by using the independent data. If interim results are not acceptable next iteration to the required step is proceeded.

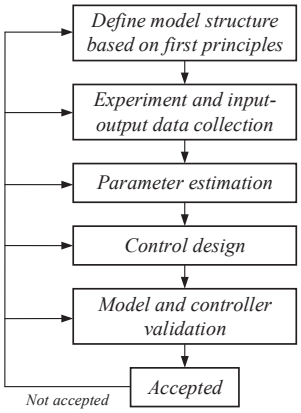

Fig. 3. System identification and control design flowchart

A. Traveling trolley approximation

Most simple way, the system plant is first modeled as a linear stage of the ball-screw drive without relative motion of the mounted pendulum. Applying the Newton's second law to the the horizontal axis x the system description is obtained as

$$F_{in} = m_C \ddot{x} + F_f. \tag{1}$$

The lumped mass m_C is that of the traveling block combined with additional weight of the pendulum. The friction force

$$F_f = c\,\mathrm{sign}(\dot{x}) + d\dot{x} \tag{2}$$

is considered as a linear combination of the Coulomb friction, with the parameter c, and viscous friction due to the grease lubrication, with the parameter d. When neglecting the nonlinear Coulomb friction contribution, eq. (1) can be transformed into Laplace domain so as to obtain the system transfer function. The transfer function between the input force and output position of traveling block is given by

$$T(s) = \frac{X(s)}{F_{in}(s)} = \frac{1}{s}\frac{1}{m_C s + d}. \tag{3}$$

B. Parameters estimation

A frequency analysis of the system is performed using the spectrum analyzer in the frequency domain of $1\,Hz - 1\,kHz$. Spectrum analyzer is set to provide sinusoidal signals with peak amplitude of $\pm 2\,V$ throughout the frequency domain. The obtained frequency response of the system is illustrated in Fig.

4. It can be observed that the system hits its natural frequency at around $450 - 650\,rad/s$. Due to influence of the coupled dynamics (motor inertia and attached mass) it discloses a resonance-antiresonance range. Due to one free integrator of the plant model, see eq. (3), it is expected that the gain starts decaying with $-20\,dB/dec$. However, the gain starts rather with a flat range of $0\,dB/dec$ change. This can be explained

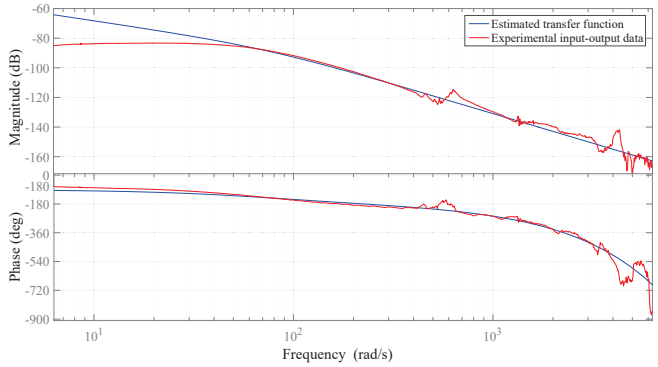

Fig. 4. Measured frequency response and plant approximation

by the impact of nonlinear friction at lower frequencies, where pre-rolling region dominates and does not allow for regular macroscopic displacements at particular sinusoidal excitation. Another significant point, observed at the sine-sweep analysis, is the affect of input voltage amplitude. The system gain and breaking frequency varied as the input amplitude varied. When rewriting the plant transfer function as following

$$T(s) = \frac{1}{s}\,\frac{1/d}{s\,m_C/d + 1}, \tag{4}$$

it can be seen that the gain is inversely dependent on the damping coefficient d. Therefore, identifying the viscous friction coefficient from the frequency response may yield inaccurate. However, the lumped mass is accurately identified in the linearly decreasing region of frequency response, for which the system description can be reduced to a double integrator, with the gain inversely proportional to the system mass, i.e.

$$T^*(s) = \frac{1}{m_C s^2}. \tag{5}$$

Note that the mass parameter has been also computed theoretically by using the catalogue and calculated values of the all moving parts, cf. in Table I.

The viscous and Coulomb friction parameters have been identified by exiting the system with trapezoidal velocity profiles. In the steady-state region, where the relative velocity is constant, the driving input force is equal to the friction force F_f. Experiments are made for a range of different velocities to obtain a complete set of friction values. Both directions are evaluated to assess irregularities and asymmetries of the friction. The friction coefficients are determined by fitting the $d\dot{x} + c$ line through the obtained points in the linear region.

All estimated parameter values are given in Table I. The comparison of estimated transfer function and measured frequency response is illustrated in Fig. 4. Note that a minor deadtime, affecting the phase response, is also identified. However, for simplicity reasons, it is excluded from the system modeling.

TABLE I. IDENTIFIED SYSTEM PARAMETERS

Friction	*Value*	*Mass*	*Value*
Coulomb friction coef. c	$17.41[N]$	*Theoretical*	$3.81[kg]$
Viscous friction coef. d	$257[Ns/m]$	*Identified*	$3.5[kg]$

C. Damping identification of swinging load

The frictional torque of the pendulum bearing can be expressed in angular coordinates φ as

$$M_f = a\,\mathrm{sign}(\dot{\varphi}) + b\dot{\varphi}. \tag{6}$$

The nominal frictional moment is estimated to be $M_f = 0.04\,Nm$. Although, the frictional moment is estimated by using an online calculator from SKF Inc, its real value – after mechanical assembly – may not match with the nominal one. Therefore, a parameter adjustment is made by using the discrete sensors, cf. Fig. 1. Initially using the nominal parameters in the numerical simulation, a pendulum drop from 90° angle has been considered and the number of zero-crossings has been counted (in the simulation) as 63 until an apparent motion stop. For comparison, the experimental setup of the pendulum has been also dropped from a well-defined 90° angle. Using the implemented discrete sensors, the number of zero-crossings has been accounted of to be about 83. Moreover, the tangential velocity of pendulum has been observed by using the combination of both discrete sensors. The sensors are mounted together with a fixed distance of $d_s = 10\,mm$ between them. Using the measured time difference Δt between both discrete impulses and geometry of sensors arrangement, the tangential velocity is observed as

$$v_t = \frac{d_s}{\Delta t}. \tag{7}$$

Using the angular velocity from the numerical simulation and the total operating length of the pendulum rod r the model-based tangential velocity is obtained as

$$\hat{v}_t = \dot{\varphi} r. \tag{8}$$

The Coulomb and viscous friction coefficients of the pendulum are adjusted so that the number of zero-crossings and the shape of decreasing instantaneous tangential velocity are possibly the same for experimental observations and numerical simulation. Both tangential velocity curves for zero-crossings are compared in Fig. 5. The identified, based thereupon, Coulomb and viscous friction coefficients are given in Table II.

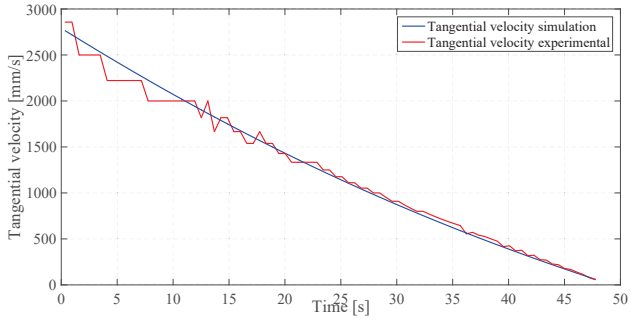

Fig. 5. Simulated and measured with discrete sensors tangential velocity

TABLE II. IDENTIFIED PENDULUM DAMPING VALUES

Coulomb friction a	*Viscous friction* b
$20[Nmm]$	$3.4[Nmms/rad]$

IV. MOTION CONTROL DESIGN

The designed position control of the traveling trolley is shown in block diagram in Fig. 6. A cascaded control architecture is used to achieve an accurate position tracking. The cascaded controller consists of an inner velocity loop and an outer position loop. Additionally, a reference velocity

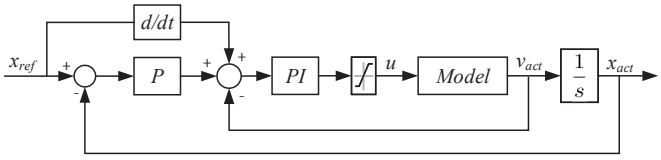

Fig. 6. Motion control architecture (simulation setup)

feed-forwarding is included to enhance the position tracking performance. For the velocity loop, a PI-controller is used so as to eliminate the steady-state error. For the position loop, a simple P-controller is used, which is however sufficient if the inner loop is accurately tuned. It is worth noting that the impact of Coulomb friction has been included when tuning the control parameters within numerical simulation. The determined controller parameters are listed in Table III.

TABLE III. CONTROLLER GAIN VALUES

Controller	*P*	*I*
Velocity loop	80	5000
Position loop	100	

The experimental evaluation of the designed controller position tracking is shown in Fig. 7. From the error plot below it can be seen that the deviation in the position tracking is relatively small and do not exceed $0.14\,mm$, even though in this experiment the system is driven with an assumed maximal relative velocity of $400\,mm/s$. The latter is assumed with respect to the motion constraints and mounted pendulum on the ball-screw drive.

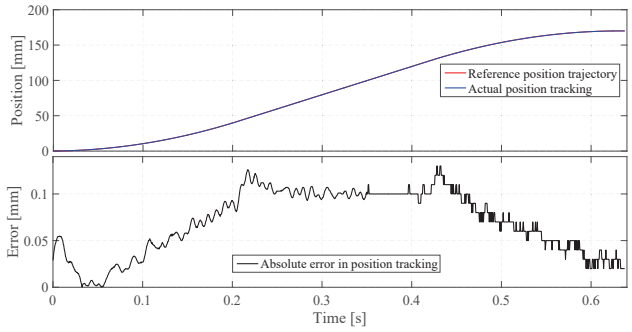

Fig. 7. Experimental evaluation of position control

V. OVERALL MODEL AND CONTROL VALIDATION

Once all model parameters are identified, the pendulum and traveling block sub-models are combined with each other in the numerical simulation. For simplicity reasons, the mass of the pendulum rod and load are combined to the total one m_L and considered as a point mass. The forces that the traveling block is subjected to are given in eq. (9), and the torques that the pendulum rod is subjected to are given in eq. (10), cf. [5]:

$$F_{in} = F_f + m_C\ddot{x} + m_L l\left(\ddot{\varphi}\cos(\varphi) - \dot{\varphi}^2\sin(\varphi)\right), \quad (9)$$

$$0 = m_L l\cos(\varphi)\ddot{x} + m_L l^2\ddot{\varphi} + m_L g l\sin(\varphi) + M_f, \quad (10)$$

with

$$M_f = a\,\mathrm{sign}(\dot{\varphi}) + b\,\dot{\varphi} \quad \text{and} \quad F_f = c\,\mathrm{sign}(\dot{x}) + d\,\dot{x}.$$

Experiments have been carried out by using the discrete sensors to analyze the response and validate the overall system model. Smooth second-order polynomial trajectory has been used for position tracking. This includes smooth start and stop of the traveling block. The discrete sensor is used to capture the time instant and number of zero-crossings of the pendulum at the stop position. The control output is also recorded during the experiment. Afterwards, the real (measured) control output is used as an excitation signal within numerical simulation, in order to examine the model response and compare it with experiments. The time instants of the zero-crossing, recorded by the discrete sensor, are shown in Fig. 8 over the simulated swinging of the excited pendulum. Recall that in the experiments, no angular encoder measuring the rotary pendulum motion is available, and only the discrete observations of zero-crossing can be used. It can be seen that the time instants of zero-crossing of experiment and simulation coincide quite well with each other. However, within the simulation the pendulum oscillates about two periods longer than the real system. This can be explained by the sticking and certain dead-zone in the bearing, which are not included into the simulated model.

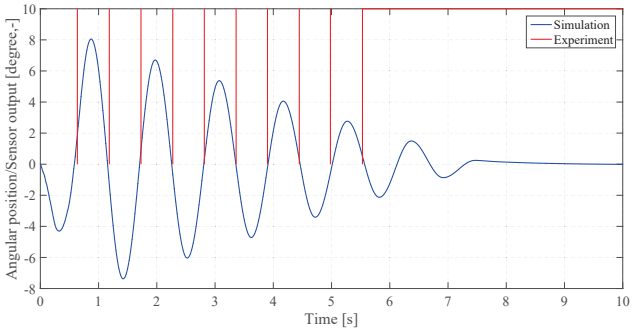

Fig. 8. Time instants of zero-crossings, experiment versus simulation

As visible from the above equations, both dynamics – of the traveling block and pendulum – are coupled and therefore additionally exciting each other. However initially, the traveling block and controller have been modeled without considering the coupling forces. Therefore, these additional forces act as a disturbance, from the controllers' point of view. An experiment is carried out to examine the performance of controller in presence of pendulum-related disturbance of a larger magnitude. The experiment consists of tracking the same smooth trajectory, however, with the pendulum initially exited by a large angle of amplitude e.g. free drop. Figure 9 illustrates the output of controller with a 'regular' run (pendulum not excited) and when the pendulum is artificially

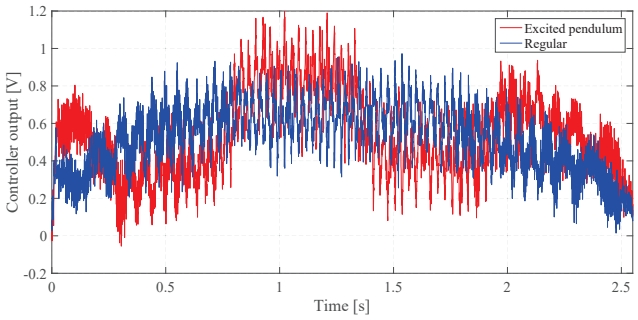

Fig. 9. Controller output, unexcited versus additionally excited pendulum

excited. The controller is affected by the added disturbance to some extent. At the same time, as disclosed in Fig. 10, the position tracking is not much affected by the disturbance, that argues for robustness of the designed motion controller.

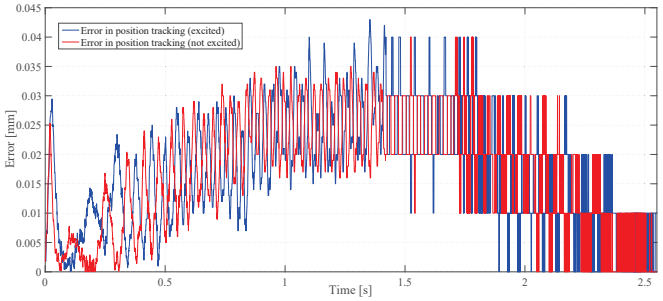

Fig. 10. Position error, unexcited versus additionally excited pendulum

Another crucial point to be analyzed is how far the swinging pendulum effects the eigen-dynamics of traveling block. This is, particularly, of an interest since it can be desirable to design an observer which will reconstruct the position of pendulum based on the measured states of the traveling block. Figure 11 illustrates the position of the traveling block

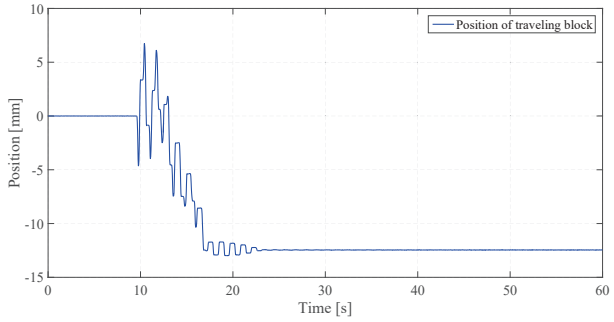

Fig. 11. Excited position of traveling block due to pendulum oscillations

when the pendulum is dropped from the horizontal position (maximal swinging amplitude), at time 10 sec, with the controller deactivated. It can be observed that at high amplitudes of swinging pendulum the traveling block dynamics is affected. However, during normal operations the amplitudes are much smaller and do not induce the motion of the traveling block sufficiently for a reliable states observation. Therefore, due to a high damping in the guide-way and small amplitude angles, oscillations of the traveling block caused by the coupling with pendulum are negligible. Hence, reconstructing the position of pendulum from the measured motion of traveling block yields as barely realizable.

Effect of varying payload on system dynamics

Effect of the load reduction on the motion control performance and pendulum dynamics have been examined by reducing the load by 50%. The results of corresponding experiment are summarized in Table V. By reducing the load to $0.5\ kg$, a 21% reduction in the overshoot percentage and slightly improvement in the settling time are obtained. However, the load also affects the pendulum dynamics drastically. The load reduction causes almost 41% less zero-crossings when dropping from the horizontal position. This appears as quite natural since during the twice reduction of inertial torques the frictional damping torques remain almost the same.

TABLE IV. AFFECT OF VARYING LOAD

Load	***1*** $[kg]$	***0.5*** $[kg]$	***Difference*** $[\%]$
Overshoot $[\%]$	5.9	4.5	-24
Settling time $[s]$	0.067	0.063	-6
Zero-crossing $[-]$	86	52	-40

VI. EVENT-BASED HYBRID CONTROL AND OSCILLATION REDUCTION

In order to reduce the operation time, i.e. time of the load positioning, the system should operate with relatively high velocities and the oscillations should be minimized at the same time. Because of discontinuity in acceleration of the second-order polynomial trajectories it will be spikes in the jerk, which can serve as additional excitation of the swinging load. Therefore, a fourth-order polynomial trajectory based on the jerk limitation has been designed to further examine the effect of oscillations. The simulation results of the load oscillation for two given trajectory profiles are illustrated in Fig. 12. It can be seen that the 4-th order polynomial trajectory does not lead to real reduction of the load oscillations, and already the 2-nd order motion trajectory can be assumed as sufficient.

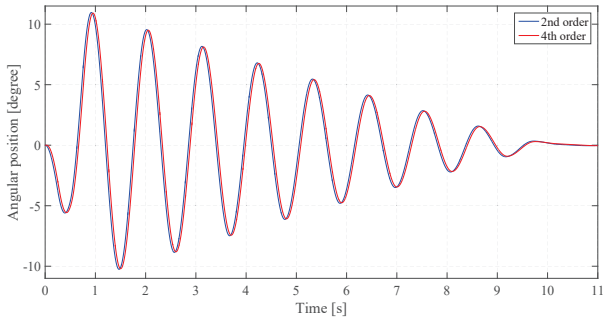

Fig. 12. Pendulum oscillation for different-order position trajectories

As can be recognized from eq. (10), the main factor which causes oscillations is acceleration of the traveling block. The affect of acceleration on the oscillation of pendulum is further analyzed along with evaluation of the event-based hybrid control. The experiment consists of driving the system with a prescribed motion profile. Using the discrete-event signal from

the digital sensor, the traveling block should start to decelerate smoothly and then return back to the position where the event-based impulse has been detected. Note that the deceleration and returning trajectories are computed in real-time. This allows for freely placing the discrete external sensors, hence generating/adapting the event-based positioning trajectory.

The experimental evaluation of the event-based hybrid control is shown in Fig. 13. It can be seen that after the discrete-signal triggering the traveling block decelerates smoothly and returns back to the position where the discrete-event happened. Also both discrete sensors have been used

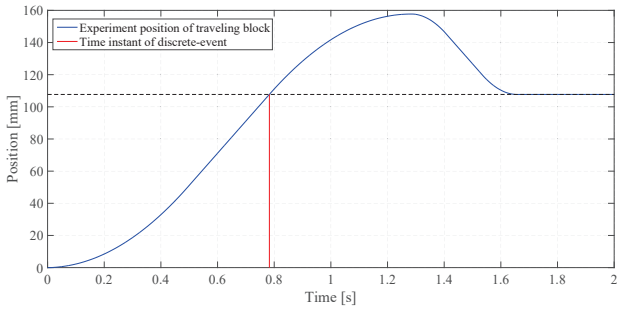

Fig. 13. Experimental evaluation of event-based hybrid control

to capture the number of zero-crossings at the final position, which gives measures of the residual load oscillations. The experiments have been carried out for sensors placed at two different distances, once at approximately $100\ mm$ and once at approximately $250\,mm$ from the starting point. In addition, the cart acceleration has been varied to see how it affects the number of oscillations.

The number of zero-crossings as function of the acceleration is shown in Fig. 14. Although, the oscillations are highly

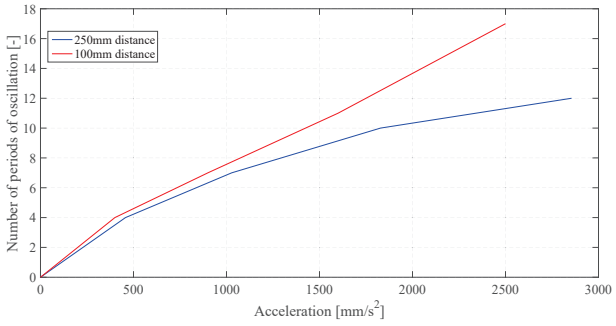

Fig. 14. Number of zero-crossings as function of cart acceleration

dependent on the maximum acceleration of traveling block, the operating distance is also affecting the oscillations. In fact, even though the system is subject to higher acceleration, the number of zero-crossing is less for the longer distance to discrete-event. This is because at longer distance, the traveling block runs longer with a constant velocity, and the initially excited oscillations disappear before the discrete-event occurs. This is not a case for the shorter distance. All things considered, one can conclude that to keep the oscillation low as possible one should also consider the length of the operation (positioning) distance. For the longer distances, the system can be exited with the relatively high accelerations. However, for shorter distances, the acceleration should be kept in the range of $500 - 1000\,mm/s^2$, where the number of oscillations is approximately the same for the short and long range under evaluation.

VII. Conclusions

This paper introduced a novel experimental framework of the traveling trolley with swinging load aimed for investigation of the hybrid motion control methods. The traditional problem of an under-actuated payload, similar to the cart with pendulum, has been considered from a point of view when the pendulum states are not directly measurable and the continuous dynamic quantities of the traveling block (cart) only are available. The introduced additional (contactless) discrete sensors proved to be suitable for an impulse-based detection of the swinging load position and estimation of its tangential, correspondingly angular, velocity at zero-crossings. The mechatronic design of experimental setup allowed for its accurate identification and development of control for the cart position tracking. The coupling effects between the cart and swinging load dynamics have been analyzed and evaluated with experiments. The first simple event-based hybrid control strategy has been designed and evaluated for the unknown final position of traveling trolley with objective of reducing the undesired swinging of the load. The developed and implemented experimental framework allows for further research on hybrid control systems, like for example [11], in terms of using less expensive and robust discrete sensors decoupled from the plant.

References

[1] W. M. Haddad, V.-S. Chellaboina, and S. G. Nersesov, *Impulsive and Hybrid Dynamical Systems: Stability, Dissipativity, and Control*. Princeton University Press, 2006.

[2] J. Lunze and F. Lamnabhi-Lagarrigue, *Handbook of hybrid systems control: theory, tools, applications*. Cambridge University Press, 2009.

[3] X. D. Koutsoukos, "Estimation of hybrid systems using discrete sensors," in *IEEE 42nd Conference on Decision and Control (CDC2003)*, 2003, pp. 155–160.

[4] H.-H. Lee, "Modeling and control of a three-dimensional overhead crane," *ASME Journal of dynamic systems, measurement, and control*, vol. 120, pp. 471–476, 1998.

[5] A. Piazzi and A. Visioli, "Optimal dynamic-inversion-based control of an overhead crane," *IEE Proceedings-Control Theory and Applications*, vol. 149, no. 5, pp. 405–411, 2002.

[6] G. Bartolini, A. Pisano, and E. Usai, "Second-order sliding-mode control of container cranes," *Automatica*, vol. 38, no. 10, pp. 1783–1790, 2002.

[7] Y. Fang, W. Dixon, D. Dawson, and E. Zergeroglu, "Nonlinear coupling control laws for an underactuated overhead crane system," *IEEE/ASME transactions on mechatronics*, vol. 8, no. 3, pp. 418–423, 2003.

[8] L. Ramli, Z. Mohamed, A. M. Abdullahi, H. Jaafar, and I. M. Lazim, "Control strategies for crane systems: A comprehensive review," *Mechanical Systems and Signal Processing*, vol. 95, pp. 1–23, 2017.

[9] Y. Yoshida and K. Tsuzuki, "Visual tracking and control of a moving overhead crane load," in *IEEE 9th International Workshop on Advanced Motion Control (AMC2006)*, 2006, pp. 630–635.

[10] M. Ruderman and M. Iwasaki, "Analysis of settling behavior and design of cascaded precise positioning control in presence of nonlinear friction," in *International Power Electronics Conference (IPEC-Hiroshima 2014-ECCE-ASIA)*, 2014, pp. 1665–1670.

[11] M. Ruderman, "Impulse-based hybrid motion control," in *IEEE 43rd Annual Conference of the Industrial Electronics Society (IECON2017)*, 2017, pp. 4049–4054.